International Journal of Refrigeration 164 (2024) 243–256

Contents lists available at ScienceDirect

International Journal of Refrigeration

journal homepage: www.elsevier.com/locate/ijrefrig

Experimental investigations of upscaling effects of high-temperature heat pumps with R1233zd(E)

Études expérimentales des effets de mise à l'échelle des pompes à chaleur haute température au R1233zd(E)

Jaromir Jeßberger [a,*], Cordin Arpagaus [b], Florian Heberle [a], Leon Brendel [b], Stefan Bertsch [b], Dieter Brüggemann [a]

[a] Chair of Engineering Thermodynamics and Transport Processes (LTTT), Center of Energy Technology (ZET), University of Bayreuth, Germany
[b] Eastern Switzerland University of Applied Sciences, Institute for Energy Systems (IES), Buchs, Switzerland

ARTICLE INFO

Keywords:
High-temperature heat pump
Upscaling
Experimental investigation
Low-GWP
Comparison

Mots-clés:
Pompe à chaleur à haute température
Mise à l'échelle
Étude expérimentale
Faible PRP
Comparaison

ABSTRACT

High-temperature heat pumps (HTHP) are crucial for decarbonizing district heating and industry. Hence, a reliable performance estimation considering effects of scaling is of interest for cost-efficient system integration. This study compares two laboratory HTHPs with the same refrigerant R1233zd(E). These systems have a similar plant design but a capacity scale factor of 3.2. The aim is to evaluate scale effects and make general valid statements about the challenges of upscaling laboratory test results. The analyses show that it is essential to distinguish between design effects like temperature differences at the pinch point or different heat exchanger surfaces and scale effects like relative heat losses and efficiencies of components and the system. At the component level, large surface reserves in the heat exchangers lead to 3–5 K smaller approach temperature differences in the lower capacity HTHP. At the system level, the relative heat losses are about 15 % higher than in the system with a larger capacity. The coefficient of performance of both HTHPs shows a similar trend as a function of the temperature lift from the heat source to the sink. Cross-referencing these performance results with over 200 data points from the literature, validated the possibility of upscaling.

1. Introduction

Addressing global warming is a paramount challenge of our time. However, the utilization of renewable energy sources in the European heating sector remains relatively low, accounting for only around 21 % in 2018, despite this sector representing over 50 % of European final energy consumption (World Energy Council, 2020). Integrating high-temperature heat pumps (HTHPs) into renewable energy systems holds great promise for a sustainable and resource-efficient supply of thermal energy. HTHPs can be applied in various ways, such as in geothermal systems or enhancing waste heat recovery from industrial processes. By incorporating HTHPs, it becomes possible to ensure sustainable coverage of peak loads, supply process heat, and upgrade the thermal capacity of district heating networks. This means the system can be used flexibly and in various sizes, e.g., in small decentralised or large-scale systems such as district heating networks. Therefore, the challenge is integrating these systems in terms of efficiency and flexibility depending on the power output in system simulations or designs.

The definition of the term HTHP is vague. For instance, Arpagaus et al. (2018) categorized heat pumps with supply temperatures exceeding 100 °C as HTHP systems. On the other hand, the International Energy Agency (2014) defined HTHP as classic industrial heat pumps with a heat source temperature of up to 40 °C and a heat sink temperature of up to 80 °C. They propose using the term "very-high-temperature heat pumps" for heat sink temperatures surpassing 100 °C. This study follows the classification of IEA without differentiating between very-high-temperature heat pumps and HTHPs.

The number of publications on HTHPs is increasing (Web of science 2022) (see Fig. 1) as are the review articles.

Bamigbetan et al. (2017) identified the current challenges for research in refrigerant selection, innovative refrigerant mixtures and

* Corresponding author.
E-mail address: jaromir.jessberger@uni-bayreuth.de (J. Jeßberger).

https://doi.org/10.1016/j.ijrefrig.2024.04.023
Received 18 January 2024; Received in revised form 2 April 2024; Accepted 26 April 2024
Available online 27 April 2024

Nomenclature

A	Heat exchanger surface m^2
CFC	Chlorofluorocarbon -
COP	Coefficient of performance -
cp	Specific heat capacity J kg^{-1} K^{-1}
FS	Full-scale uncertainty%
GWP	Global warming potential CO_2e
h	Enthalpy J·kg^{-1}
HCFO	Hydrochlorofluoroolefine -
HFC	Hydrofluorocarbon -
HCFC	Hydrochlorofluorocarbon -
HFO	Hydrofluoroolefine -
HTHP	High-Temperature Heat Pump -
IHX	Internal heat exchanger -
$\dot{m}$	Mass flow rate kg s^{-1}
n	Compressor speed 1 s^{-1}
ODP	Ozone depletion potential R-11e
OR	Operating range uncertainty%
p	Pressure bar
P	Electrical power kW
POE	Polyolester -
Pr	Prantl number -
$\dot{Q}$	Thermal capacity kW
r	Inner radius of cylinder m
Re	Reynolds number -
s	Piston stroke m
T	Temperature °C
TFA	Trifluoroacetic acid -
U	Overall heat transfer coefficient W m^{-2} K^{-1}
V	Volume flow rate m^3 s^{-1}
z	Number of cylinders -
α	Heat transfer coefficient W m^{-2} K^{-1}
ΔT	Temperature difference K
Δx	Sensor uncertainty%
Δy	Combined uncertainty%
η	Efficiency -
λ	Thermal conductivity W m^{-1} K^{-1}

Subscripts

1 – 9	State points -
calc	Calculated values -
Carnot	Carnot efficiency -
comp	Compressor -
cond	Condenser -
heat sink	Heat sink -
inlet	Inlet of a heat exchanger -
isen	Isentropic -
lift	Lift -
Lorentz	Lorentz efficiency -
loss	Heat losses -
m	Mean -
measured	Measured values -
MITA	Minimum temperature approach -
outlet	Outlet of a heat exchanger -
sink,out	Heat sink outlet -
source,in	Heat source inlet -
th	Theoretical -
vol	Volumetric -

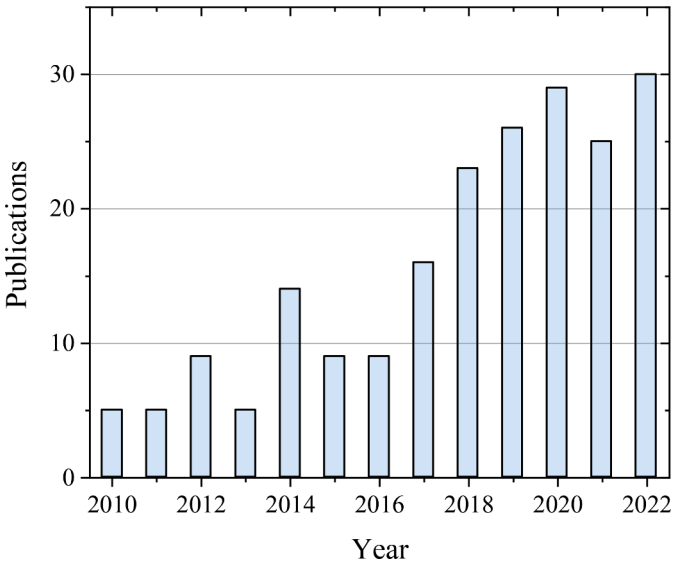

Fig. 1. Number of "high temperature heat pump" publications over the year (based on Web of Science data (Web of science 2022)).

cascade systems. In particular, they mentioned the need to investigate higher pressure ratios and compressor cooling. Arpagaus et al., 2018) emphasized the need to minimize heat losses, oil lubrication and to investigate scale up for industrial applications. Adamson et al. (2022) identified the great potential of transcritical systems and formulated six challenges with the corresponding solution proposals. Sun et al. (2023) and Jiang et al. (2022) added an increase in efficiency at high-temperature lifts and the development of large-scale HTHPs above 1 MW thermal capacity. Khalid et al. (2023) also focused on improving the compressors and optimizing heat transfer through tighter mean temperatures and oil-free operation. All review papers (Arpagaus et al., 2018, Bamigbetan et al., 2017, Adamson et al., 2022, Sun et al., 2023, Jiang et al., 2022, Khalid et al., 2023) showed that piston compressors are often used in HTHPs, and the state-of-the-art heat pump cycle designs include internal heat exchangers.

Developments in different fields are reached in the heat pump market, and the manufacturers regularly present new prototypes. To name a few, ecop Technologies GmbH (Austria) is working on a high-temperature rotation heat pump with a refrigerant mixture of argon, helium and krypton (Längauer and Adler, 2023). The manufacturer Sustainable Process Heat GmbH (Germany) developed a new reciprocating compressor with an improved valve system and heat management (Hamacher, 2022). Enerin AS (Norway) presented a new "ultra-high temperature heat pump" based on the Stirling cycle with helium as a working fluid (Høeg et al., 2023) in 2023. Recently, MAN presented a CO_2-heat pump with a thermal capacity of 50 MW (Decorvet, 2023). There are numerous other developments in the market which are summarized by Arpagaus et al. (2018). In addition to the scientific studies, this short overview presents aspects of the HTHP market illustrates many significant development approaches. Besides the selection of the refrigerant and the improvement of the component performance, another challenge is the upscaling of the systems, which is an important aspect in the interpretation and processing of the test results. With respect to the refrigerant, chlorofluorocarbons (CFCs) and hydrochlorofluorocarbons (HCFCs) may no longer be used in new plants due to their high ozone depletion potential (ODP) since the implementation of the Montreal Protocol (European Union, 1991) in 1991. Both heat pumps and refrigeration systems were operated using hydrofluorocarbons (HFCs) such as R245fa (1,1,1,3,3-Pentafluorpropan) for

many years, but the high global warming potential (GWP) of the HFCs lead to the so-called F-Gas-Regulation (European Union, 2014), which implements a phase-down of fluorinated greenhouse gases in the EU. Due to these legal restrictions, synthetical refrigerants with low GWP were introduced to the market. Examples are hydrofluoroolefins (HFOs) such as R1336mzz(Z) ((Z)-1,1,1,4,4,4-hexafluor-2-buten) and R1234yf (2,3,3,3-tetrafluorpropen) but also hydrochlorofluoroolefins (HCFOs) such as R1233zd(E) (trans-1-chloro-3,3,3-trifluoropropene) and R1224yd(Z) (cis-1-chloro-2,3,3,3-tetrafluoropropene). The advantages of HCFOs and HFOs compared to natural refrigerants are the consistent requirements for the installation and the safety engineering of HFCs. One disadvantage is the formation of trifluoroacetic acid (TFA) as an atmospheric degradation product when some types of HCFOs and HFOs are released into the environment. In Europe, HFO and HCFO refrigerants may therefore be phased out in the near future. However, the literature research reveals that the HCFO R1233zd(E) performs exceptionally well in HTHP cycles and is a commonly used refrigerant in high temperature applications, so it is used in this study. For example, Mateu-Royo et al. (2019) theoretically evaluated different refrigerants in a HTHP cycle with the result that R1233zd(E) leads to an increase of 27 % in the coefficient of performance (*COP*) compared to R245fa and compared to other synthetic refrigerants to the highest potential CO_2 reduction. Arpagaus et al. (Arpagaus et al.; Bamigbetan et al., 2018; Arpagaus and Bertsch, 2021; Arpagaus and Bertsch, 2019; Arpagaus and Bertsch, 2020), Frate et al. (2019), Bamigbetan et al. (2018) and Chen and Kyung Kwon (2022) showed similar results. Due to its significantly high critical temperature of 166.5 °C (climalife), R1233zd(E) enables high discharge and supply temperatures, distinguishing it from other refrigerants. Only a few HFOs have a higher critical temperature, for example, R13336mzz(Z) with 171.3 °C (Konstantinos Kontomaris, 2014). R1233zd(E) has a GWP of 1 CO_2-eq. and due to the chlorine content, an ODP of 0.000034 CFC-11-eq. (IPCC, 2014).

Table 1 summarizes recent experimental studies (2019 to 2023) where R1233zd(E) is experimentally investigated as the refrigerant in a HTHP system.

The listed publications in Table 1 show the results of the different test rigs in changing operational conditions or concepts, like:

- the use of an internal heat exchanger leads to an increase of the *COP* (Arpagaus and Bertsch, 2021; Arpagaus and Bertsch, 2020; Arpagaus et al., 2019),
- with decreasing compressor speed the *COP* is increasing during part load operation (Jeßberger et al., 2022b; Hassan et al., 2022) and
- R1233zd(E) shows a better performance than R245fa (Chen and Kyung Kwon, 2022; Shah et al., 2019).

These studies commonly focus on a single experimental facility and validate the measured experimental results using simulation models or literature data. Nevertheless, given the considerable disparity between these experimental setups and industrial-scale operations, an important research question arises regarding the feasibility of directly upscaling the laboratory results to a larger thermal capacity.

This research gap motivates the present study, where the 11 kW HTHP presented by Arpagaus and Bertsch (2019) is compared to the 35 kW HTHP published by Jeßberger et al. (2022b) on system and component levels at different operating points. Fundamentally, the two existing laboratory test rigs are similar in construction (i.e., heat pump cycle with piston compressor and internal heat exchanger (IHX)), which is discussed in more detail in the following chapter and enable a comparison on system and component level. The comparison focuses on evaluating the important effects of a scale-up and distinguishing scale-up and design effects. For this purpose, different operating points, published by Arpagaus and Bertsch (2019), were measured, with the same boundary conditions, at the HTHP plant published by Jeßberger et al. (2022b).

Based on these results, detailed analyses are conducted for:

Table 1
Recent experimental HTHP research projects with R1233zd(E) as refrigerant.

Author	Focus	Q_{sink}	Year
Arpagaus and Bertsch (Arpagaus and Bertsch, 2019)	• Comparison of HFO/HCFO refrigerants • 30 K to 70 K temperature lift • Supply temperature up to 150 °C	11 kW	2019
Arpagaus and Bertsch (Arpagaus et al., 2019)	• Comparison of R1233zd(E) and R1336mzz(Z) • 30 K to 70 K temperature lift • Supply temperature up to 150 °C	11 kW	2019
Shah et al. (Shah et al., 2019)	• Comparison of R1233zd(E) and R245fa • R245fa simulated • Supply temperature up to 135 °C	13.8 kW	2019
Arpagaus and Bertsch (Arpagaus and Bertsch, 2020)	• Comparison of R1233zd(E) and R1224yd(Z) • 30 K to 70 K temperature lift • Supply temperature up to 150 °C	11 kW	2020
Arpagaus and Bertsch (Arpagaus and Bertsch, 2021)	• Comparison of HFO/HCFO refrigerants • 30 K to 70 K temperature lift • Supply temperature up to 150 °C	11 kW	2021
Jeßberger et al. (Jeßberger et al., 2022b)	• Part load behaviour of HTHP • 25 K to 45 K temperature lift • Supply temperature up to 104 °C	35 kW	2022
Hassan et al. (Hassan et al., 2022)	• Part load behaviour of HTHP • Development of performance maps for pumped thermal energy storage • Condensation temperature ≥ 138 °C	22 kW	2022
Chen and Kyung Kwon (Chen and Kyung Kwon, 2022)	• Comparison of R1233zd(E) and 245fa • 66 °C to 74 °C condensation temperature • 32 °C to 38 °C evaporation temperature	9 kW	2022
Jiang et al. (Jiang et al., 2023)	• Innovative heat pump design with centrifugal compressor • 30 K to 50 K temperature lift • Supply temperature up to 100 °C	381 kW	2023

- heat transfer characteristics,
- heat losses in the different components,
- compressor efficiencies, and
- system performance (*COP*).

Finally, a relation for the upscaling of HTHPs can be given, and by using further available literature data, the analyses show, that upscaling of laboratory test results to industrial scale is possible.

2. Experimental HTHP setups and methodology

The study considers two different HTHP systems with different thermal capacities. In the following, the setups are described, and the special technical features are shown. Arpagaus and Bertsch presented the first measurements on the test rig in 2018 (Arpagaus and Bertsch, 2019; Arpagaus et al., 2018). The HTHP, named in this study as “HTHP A”, has a maximum thermal capacity of 11 kW. Fig. 2 illustrates the RI scheme and shows a picture of the test rig.

Where T are the temperature, p the pressure and $\dot{m}$ the mass flow rate sensors. In addition, the “HTHP B” system is investigated in this study, which was initially introduced in 2022 (Jeßberger et al., 2022a) and is analogous to the experimental setup presented in the work of Jeßberger et al. (2022a, 2022b). With a thermal capacity of 35 kW, HTHP B has a higher thermal capacity by a factor of 3.2. However, the subsequent sections will comprehensively describe the experimental setup. The RI scheme and a picture of HTHP B are presented in Fig. 3. In both test rigs, the piping and heat exchangers are insulated to minimize heat loss. However, the compressor in both HTHPs and the liquid collector in

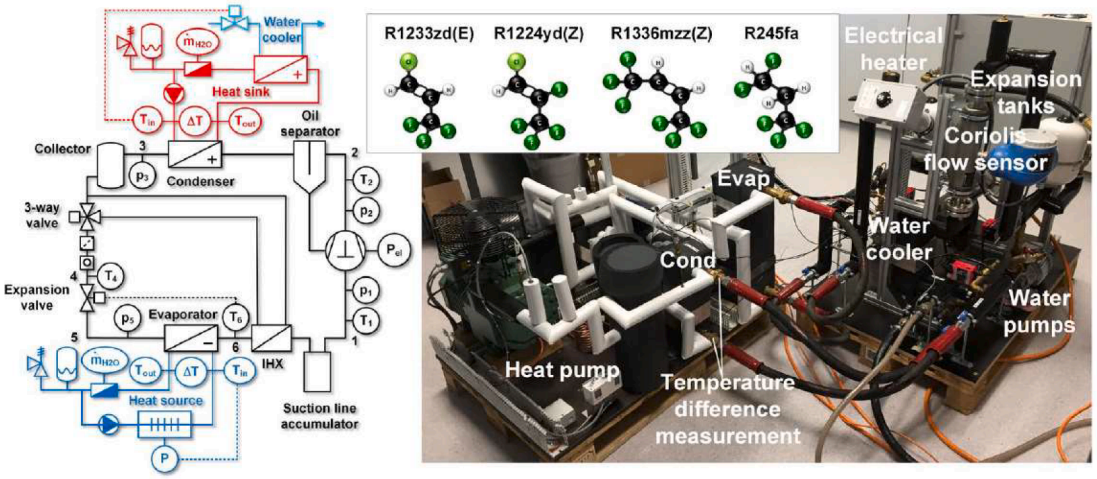

Fig. 2. RI-Scheme and picture of HTHP A (Arpagaus and Bertsch, 2021).

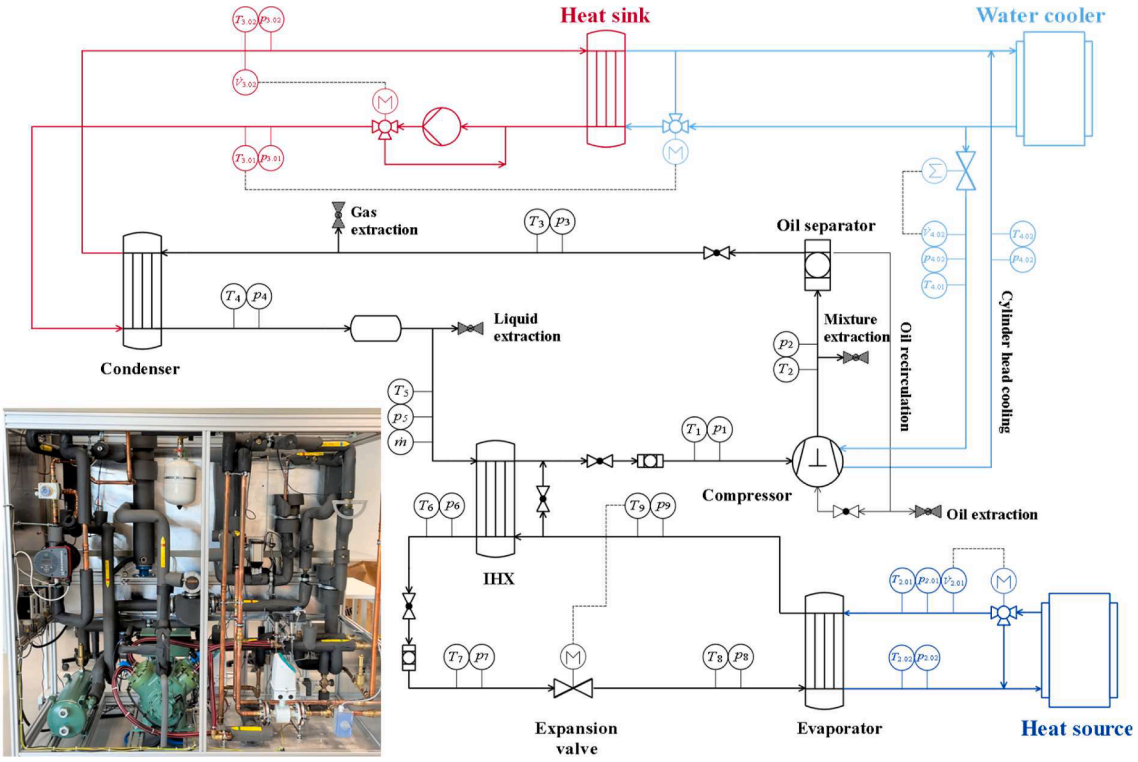

Fig. 3. RI-Scheme and picture of HTHP B.

HTHP B are not insulated due to the potential adverse effect of increased suction temperature, which could result in a reduced compressor lifetime.

The heat pumps under consideration exhibit a high degree of component similarity (see Table 2), such as a reciprocating compressor from Bitzer, plate heat exchangers and oil separator, which enables a thermodynamic comparison between them.

In the following, the heat pump circuit is generally described based on Fig. 3 and the differences between the individual systems are explained in parallel. At state point 1, the suction side of the compressor, the working medium is in a highly superheated state at a low-pressure level. Both units operate with a reciprocating compressor from Bitzer. While the compressor in HTHP A has 2 cylinders, HTHP B has 4 cylinders, thus a considerably higher power consumption and possible delivery volume. Both units work with a frequency converter to regulate the compressor's speed continuously, whereby HTHP A can be controlled between 30 Hz and 60 Hz and HTHP B between 25 Hz and 70 Hz. Additionally, the compressor of HTHP B has water-cooled cylinder heads, which can be used for waste heat recovery and reduce the discharge temperature. The working fluid is compressed, leaving the compressor at a high-temperature level at state point 2.

Both HTHPs use polyolester oil (POE), but with different viscosity levels. While HTHP A uses oil with a kinematic viscosity of 173 mm^2/s at 40 °C, the POE oil used in HTHP B has a kinematic viscosity of 80 mm^2/s at 40 °C. The potential impacts of these factors on system performance will be examined in the subsequent chapter. Since the compressor inherently carries a certain amount of oil to the discharge side, both systems use an oil separator. This component effectively separates the liquid oil from the gaseous refrigerant.

Subsequently, the refrigerant proceeds to state point 3, where it

Table 2
Comparison of the HTHP components.

Component	HTHP A	HTHP B
Compressor	2-cylinder reciprocating, Bitzer 2DES-3Y New Ecoline Delivery volume: 0.1543 L	4-cylinder reciprocating, Bitzer 4JE-22Y Delivery volume: 0.7300 L
Frequency converter	30 Hz - 60 Hz, Danfoss Vacon 100	25 Hz–70 Hz, Bitzer FOY+ 39–4
Oil separator	Temprite, Coalecent 922M	ESK-Schultze BOS2-R-35/28F
Condenser	SWEP B8LASHx30/1P-SC-M, Plate heat exchanger	SWEP B15T, Plate heat exchanger
Liquid receiver	Bitzer FS56	Bitzer F202H
Expansion valve	Siemens, MVL661.15–0.4	Danfoss, ICMTS
Internal heat exchanger	SWEP B5THx16/1P-SC-M, Plate heat exchanger	Alfa Laval CB30–34H, Plate heat exchanger
Evaporator	SWEP B25THx30/1P-SC-S, Plate heat exchanger	SWEP V80 × 40HT, Plate heat exchanger
Refrigerant quantity	4.2 kg	28 kg
Oil	POE-Oil Fuchs RenisoTriton SE 170, viscosity of 173 mm^2/s at 40 °C	POE-Oil Bitzer BSE 85 K, viscosity of 80 mm^2/s at 40 °C (FUCHS 2020)
Refrigerant	Honeywell Solstice® R1233zd (E)	Honeywell Solstice® R1233zd (E)
Thermal capacity	11 kW	35 kW

enters the condenser, transfers thermal energy to the heat sink and leaves the condenser 0 K to 3 K subcooled. The condensers utilized in both test rigs are plate heat exchangers manufactured by SWEP. From state point 4, the refrigerant enters the liquid collector, continues subcooled into the internal heat exchanger (IHX), transfers heat to the vapor stream, and ensures higher superheating. The highly subcooled refrigerant is still at high-pressure at state point 6.

With the expansion valve, the pressure drops to a level that ensures superheating of 5 K at the outlet of the evaporator (state point 9). Due to the pressure drop in the isenthalpic valve, a vapor fraction between 0.12 and 0.32 results at state point 8. The evaporator is in both test rigs, a plate heat exchanger. As a result of the increased plate count in HTHP B, a distribution device is installed to optimize heat transfer from the heat source to the refrigerant. This device needs a pressure drop of approximately 1 bar to ensure optimal heat transfer. However, this high-pressure drop is not generally obtained during part-load operation, even when the expansion valve opens very wide. Consequently, a future study will compare an evaporator with and without a distribution device to evaluate its impact. After the evaporator, the refrigerant goes through the IHX, is further superheated and enters the suction side of the compressor in state point 1. In addition, the state changes are illustrated in a log(p)-h-diagram in Fig. 4.

Different operation points with varying temperature lifts and source temperatures analogue to Arpagaus and Bertsch (2019) are evaluated to compare the heat transfer characteristics and performance of the two test rigs. The temperature lift (ΔT_{lift}) is defined as the difference between the heat sink supply temperature (state point 3.02, Fig. 3) and the inlet temperature of the heat source (state point 2.01, Fig. 3). Each operating point is measured on 3 different days to produce reliable measurement data. The mean values are then formed from the three measurement campaigns. Steady-states are defined as a change of less than 1.5 K over a period of 10 mins for the discharge temperature of the compressor and the outlet temperature of the heat sink.

The measurement uncertainties are caused by the uncertainty of sensors and of the measurement board. It is important to distinguish between a full-scale uncertainty (FS) and the operating range uncertainty (OR). FS refers to the maximum measurement deviation as a percentage of the total measurement range, while OR indicates the maximum deviation within the actual range used during a measurement. The reciprocal influence of the individual errors is calculated with the help of the Gaussian error propagation, according to DIN 1913-4 (Deutsches Institut für Normung e.V., 1999). By calculating a parameter y as a function of different parameters x_i, the combined uncertainty Δy is defined as:

$$\Delta y = \sqrt{\left(\frac{\partial y}{\partial x_1}\cdot \Delta x_1\right)^2 + \left(\frac{\partial y}{\partial x_2}\cdot \Delta x_2\right)^2 + \ldots + \left(\frac{\partial y}{\partial x_n}\cdot \Delta x_n\right)^2} \quad (1)$$

where Δx_i is the independent variable, generally provided by the manufacturer and shown in Table 3. Δx_i compromises two components: the measurement uncertainty of the sensor itself and the error introduced by the measurement board. This error propagation is indicated in the context of the *COP* error calculation (see Fig. 13).

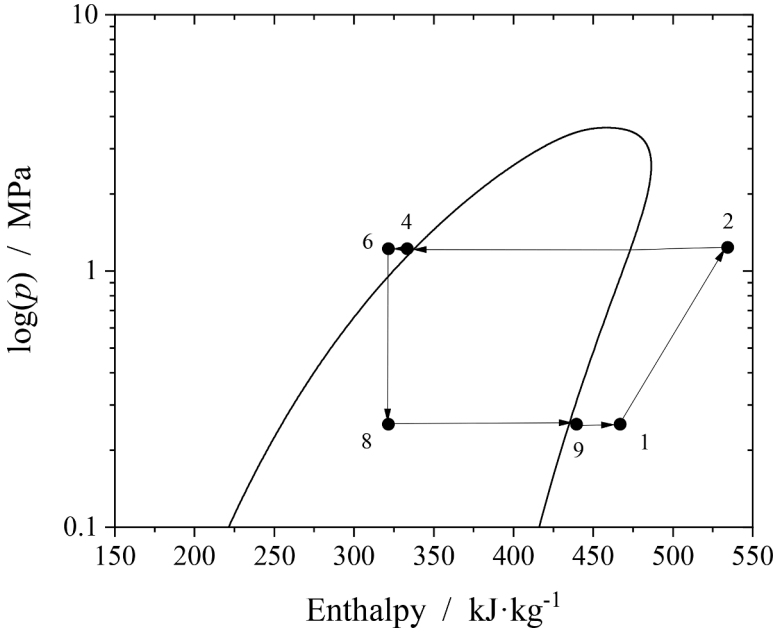

Fig. 4. log(*p*)-*h*-diagram of R1233zd(E) with the state points of the heat pump cycle.

Table 3
Sensors and uncertainties in HTHP B.

Sensor	Type	Range	Sensor uncertainty	Board uncertainty
Temperature	Omega, PR-22–3–100–1/3-M3–100-M12	-30 °C to 350 °C	$dT = \pm (1/3 \cdot (0.30\ °C + 0.005 \cdot T))$	±0.15 °C
Pressure	Omega, PAA23SY-C-5-M12, 5 bar abs.	-1 bar to 5 bar	±0.7 % FS	±0.76 %
Pressure	Omega, PAA23SY-C-20-M12, 20 bar abs.	-1 bar to 20 bar	±0.7 % FS	±0.76 %
Mass flow rate refrigerant	Endress+Hauser, Proline Promass 40E	0 kg/h to 18,000 kg/h	±0.5 % OR	negligible
Volume flow water circuits	Siemens, SITRANS FM MAG 3100 P/5100 W	–	±0.4 % OR ±1 mm/s	negligible
Electrical Power	–	–	±0.7 % OR	negligible

2.1. Measurement procedure

Arpagaus and Bertsch (2019) published experimental data for different temperature lifts from 30 K to 70 K at different source temperatures. The operating points under investigation, are shown in Fig. 5.

Due to a manufacturer limitation, HTHP B cannot operate at higher discharge temperatures than 140 °C. In consequence, only operation points published by Arpagaus and Bertsch (2019), where the discharge temperature is in this range, are evaluated in this study. Nevertheless, at three points, the discharge temperature of HTHP B reached the technical limitation, and cylinder head cooling was used to reduce the discharge temperature and protect the compressor. Arpagaus and Bertsch (2019) used operating point P9 (red) as a reference and measured it several times, the other points were measured once.

2.2. Measurements evaluation

For HTHP A, the temperature differences in the heat exchangers on the water side were kept constant at 3 K on the source side, and 5 K on the sink side using relatively high flow rates. Due to technical limitations, the differences in HTHP B were between 5 K and 10 K.

A detailed thermodynamic analysis on the component level is conducted for the heat exchangers and the compressor of each system. The compressors are examined regarding isentropic and volumetric efficiency and heat losses. The isentropic efficiency η_{isen} is defined as:

$$\eta_{isen} = \frac{\dot{m}_{refrigerant} \cdot (h_{2s} - h_1)}{P_{comp}} \tag{2}$$

where h_1 is the enthalpy at state point 1 and h_{2s} the isentropic enthalpy at the discharge side of the compressor. P_{comp} is the electrical input power, and $\dot{m}_{refrigerant}$ is the mass flow rate of the refrigerant. The volumetric efficiency of the compressor indicates the ratio between the volume flow of the refrigerant and the theoretical possible volume flow. The theoretical volume flow can be calculated with manufacturer data as shown in Eq. (3):

$$\dot{V}_{th} = z \cdot \pi \cdot r^2 \cdot s \cdot n \tag{3}$$

where z is the number of cylinders, r is the inner radius of the cylinder, s is the piston stroke, and n is the rotation speed. Accordingly, the volumetric efficiency is calculated by:

$$\eta_{vol} = \frac{\dot{V}_{refrigerant}}{\dot{V}_{th}}. \tag{4}$$

The heat losses of the compressor can be described by:

$$\dot{Q}_{comp,\ loss} = \dot{m}_{refrigerant} \cdot \left(h_{2,\ calc} - h_{2,\ measured}\right), \tag{5}$$

under consideration of the isentropic efficiency and measurement data:

$$\eta_{isen} = \frac{(h_{2s} - h_1)}{(h_{2,calc} - h_1)} \tag{6}$$

where the specific enthalpy at state point 2 is calculated with Eq. (2) and Eq. (6):

$$h_{2,\ calc} = \frac{P_{comp}}{\dot{m}_{refrigerant}} + h_1. \tag{7}$$

Because no mass flow rate sensor was installed in the refrigeration circuit of HTHP A. In this context, a medium heat loss of 10 % regarding the thermal output of the HTHP is assumed for further calculations. Based on this, the refrigerant mass flow rate in HTHP A is estimated by the energy balance of the condenser. The heat exchangers are evaluated regarding the minimum temperature approach (ΔT_{MITA}), the heat transfer capacity, the heat rate, the heat losses and temperature glide on the waterside. The minimum temperature approach describes the minimum difference between the two flows in a heat exchanger and is a design criterion for evaluating existing systems. Fig. 6 illustrates a temperature profile of the condenser in counterflow operation.

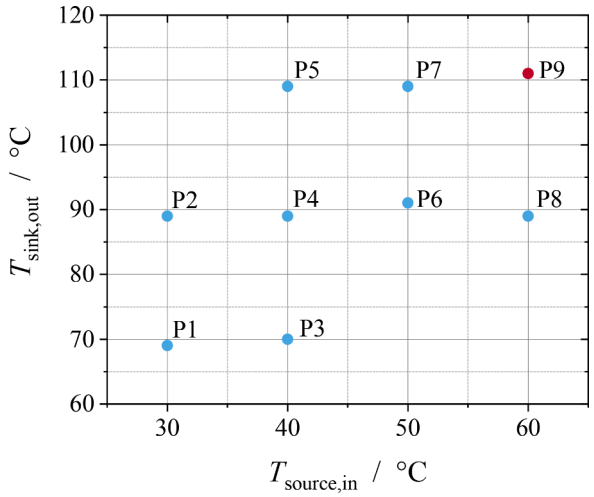

Fig. 5. Operating points under investigation.

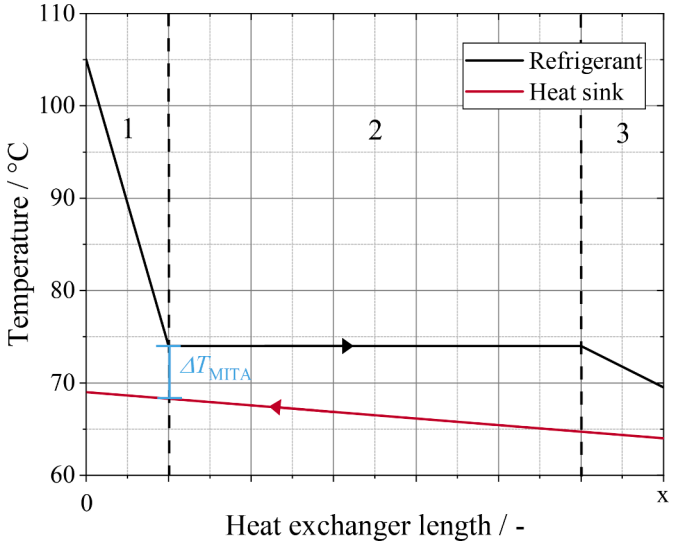

Fig. 6. Temperature profile of a condenser in counterflow operation.

The overall heat transfer coefficients U of the condenser and evaporator are determined to evaluate the heat transfer characteristics. U is calculated from the heat exchanger surface A, the thermal capacity Q and the logarithmic mean temperature difference of the heat exchanger (see Eq. (8)). Due to the phase change in the condenser the calculation of the logarithmic mean temperature difference needs to be split in three parts (see Eq. (9)). So, the overall heat transfer coefficient U leads to:

$$U = \frac{\dot{Q}_{\text{cond}}}{A \cdot \Delta T_{\text{m,log,cond}}} \tag{8}$$

with

$$\Delta T_{\text{m,log,cond}} = \frac{\dot{Q}_1}{\dot{Q}_{\text{cond}}} \cdot \Delta T_{\text{m,log,1}} + \frac{\dot{Q}_2}{\dot{Q}_{\text{cond}}} \cdot \Delta T_{\text{m,log,2}} + \frac{\dot{Q}_3}{\dot{Q}_{\text{cond}}} \cdot \Delta T_{\text{m,log,3}} \tag{9}$$

where part 1 is the superheated part of the refrigerant, part 2 is the phase change, and part 3 is the subcooling. U can also be calculated by using the heat transfer resistances in the heat exchanger:

$$U = \frac{1}{\frac{1}{htc_{\text{refrigerant}}} + \frac{s_{\text{wall}}}{\lambda} + \frac{1}{htc_{\text{water}}}} \tag{10}$$

Where htc is the heat transfer coefficient of the fluids, s_{wall} the plate thickness and λ the thermal conductivity. htc is a function of the properties of the substance, presented by the Prantl number (Pr) and the flow characteristics and geometric data presented by the Reynolds number (Re). To investigate the behaviour of the overall heat transfer coefficient, the htc-values are calculated theoretically at one specific point in the condensers, at complete condensation. For this purpose the heat exchanger design tool "DThermX" from SWEP (DThermX) is used, in which all geometric boundary conditions of the heat exchangers are implemented. Using the geometrical data of the condensers the flow characteristics and substance properties, Re and Pr can be calculated and the dominating effect for the overall heat transfer coefficient can be identified.

Due to the highest temperature difference, to the ambient, in the condenser, its heat losses have the greatest impact of all heat exchangers. Thus, the study will be focused on the heat losses in the condenser and in the compressor, which can be calculated as follows:

$$\dot{Q}_{\text{cond, loss}} = |\dot{Q}_{34}| - |\dot{Q}_{\text{heat sink}}| \tag{11}$$

with

$$\dot{Q}_{34} = \dot{m}_{\text{refrigerant}} \cdot (h_4 - h_3) \tag{12}$$

and

$$\dot{Q}_{\text{heat sink}} = \dot{m}_{\text{heat sink}} \cdot c_p \cdot \left(T_{\text{sink,out}} - T_{\text{sink, in}}\right). \tag{13}$$

The relative losses are related to the thermal capacity of the HTHP $Q_{\text{heat sink}}$. Analogues the heat losses on the system level are calculated. The most important value to evaluate the system performance of a HTHP at a specific operating point is the COP, as well as the ratio between real COP and theoretical possible COP. The theoretical COP can be described as the Carnot COP or the Lorentz COP. The Carnot efficiency is related to the inlet temperatures of the heat source and the outlet temperature of the heat sink (temperatures in Kelvin):

$$COP_{\text{Carnot}} = \frac{T_{\text{sink,out}}}{T_{\text{sink,out}} - T_{\text{source,in}}}. \tag{14}$$

By using the Carnot efficiency, the inlet and outlet temperatures of the water circuits need to be constant to compare two heat pumps. The Lorentz COP takes the temperature glide of the water circuits into account so that it is related to the logarithmic mean temperatures of the water flows and thus also represents different evaporation temperatures caused by a larger temperature glide:

$$COP_{\text{Lorentz}} = \frac{\Delta T_{\text{m,log, sink}}}{\Delta T_{\text{m,log, sink}} - \Delta T_{\text{m,log, source}}} \tag{15}$$

with

$$\Delta T_{\text{m,log, sink}} = \frac{T_{\text{sink, inlet}} - T_{\text{sink, outlet}}}{ln\left(\frac{T_{\text{sink, inlet}}}{T_{\text{sink, outlet}}}\right)} \tag{16}$$

and

$$\Delta T_{\text{m,log, source}} = \frac{T_{\text{source, inlet}} - T_{\text{source, outlet}}}{ln\left(\frac{T_{\text{source, inlet}}}{T_{\text{source, outlet}}}\right)}. \tag{17}$$

The introduced COPs describe the maximum possible efficiency regarding the second law of thermodynamics. The following chapters discuss results, and generally valid statements on upscaling are made.

3. Results

In this chapter, the experimental results are presented. The focus is led on the analysis of single components and system performance. The results are then analysed for their impact on upscaling.

3.1. Performance evaluation on the component level

To understand the behaviour of the different systems, it is necessary to investigate the single components and analyse their behaviour regarding the various operation points.

3.1.1. Heat exchangers

As mentioned in the previous chapter, the temperature glide is not as constant in HTHP B as in HTHP A because of the limitation of the water mass flow rates. As shown in Fig. 7, with the increasing thermal capacity of the heat source, the water mass flow rates of HTHP B have to be increased. At the points where the cylinder head cooling (CHC) (P5, P7, P9) was used, the temperature glide decreases in fact of the lower discharge temperature.

To compare both systems, it is important to note that the evaporation temperature decreases with a higher temperature glide on the heat source. Fig. 8 shows the minimum approach temperature, introduced in

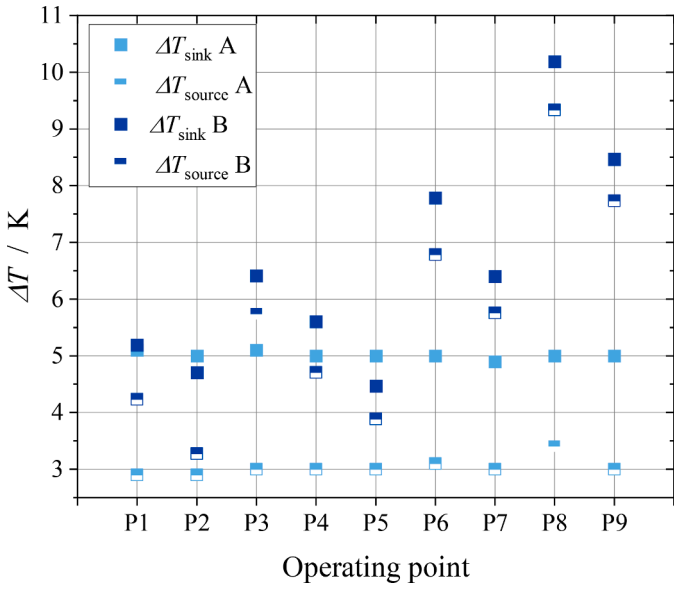

Fig. 7. Temperature glides on the heat sink and source at different operating conditions.

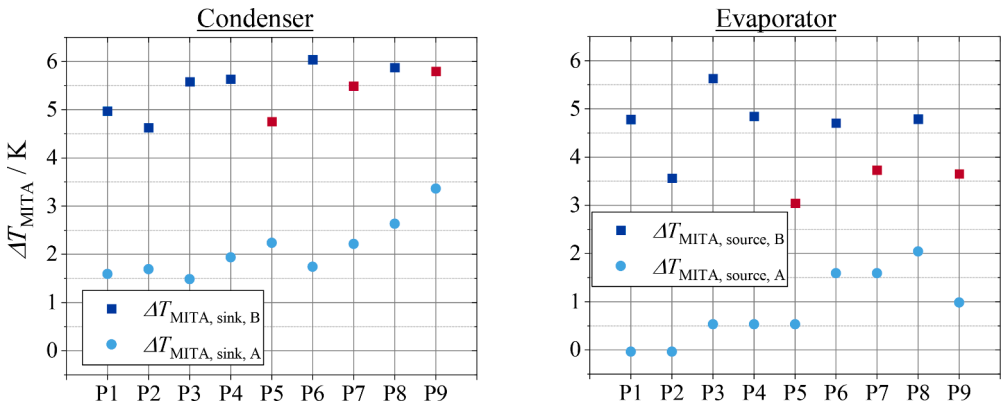

Fig. 8. Minimum temperature approach in condenser and evaporator.

Fig. 6. In the condenser of the HTHP A, the average mean ΔT_{MITA} is 2.1 K and in the evaporator 0.9 K. At measuring points P1 and P2 the refrigerant leaves with the same temperature as the water enters, which can be an indication for an oversized heat exchanger, in an economic perspective. The average mean ΔT_{MITA} in HTHP B is 5.1 K in the condenser and 4.3 K in the evaporator. When the CHC is used (red squares), ΔT_{MITA} is generally lower, because less heat must be rejected allowing a small approach temperature. Also, the higher temperature glide in the evaporator leads to a lower evaporation temperature in the HTHP cycle B (compare *Fig. 7*).

In this context, the condensation and evaporation temperatures are shown in Fig. 9. As expected from the lower ΔT_{MITA} (see Fig. 8), the evaporation and condensation temperatures of HTHP A are closer to the inlet temperatures of the heat source and sink compared to HTHP B. However, Fig. 9 shows clearly the same quantitative behaviour for both systems. The absolute deviation between the condensation temperature is 3.5 K and 5.1 K for the evaporation temperature. This is explained by the varying operating conditions of the heat sink and heat source and the different heat transfer characteristics.

Fig. 10 shows the overall heat transfer for the condenser and evaporator as a function of the temperature lift of the system. The condensers show similar trends of the overall heat transfer coefficients, namely a decrease with increasing temperature lift. A low logarithmic medium temperature has an increasing influence on U_{cond} (compare Eq. (8)). On average, a value of 5.1 K is obtained for system HTHP A compared to HTHP B with 8.6 K. Chapter 1.2 describes the calculation of heat transfer coefficients using DThermX software. The overall heat transfer coefficient, calculated by DThermX, is in medium 28 % lower in HTHP A compared to HTHP B. The difference to the experimental results may be due to heat losses that have not been considered. The heat transfer coefficient of the water side at the condenser is six times higher than that of the refrigerant, indicating that the heat transfer resistance of the water side plays a minor role. However, the heat transfer coefficient on the water side is 14 % lower for HTHP A than for HTHP B. Similarly, on the refrigerant side, the difference is 13 %. In order to highlight the effects which, lead to lower *U*-values in case of high temperature lifts, *Re* and *Pr* are analysed at the complete condensation in the condenser. The *Pr* of HTHP A is on average 1.2 % greater than that of HTHP B, which shows only minor influence of material properties. In HTHP A, *Re* at the refrigerant side is, on average, 71 % smaller than in HTHP B. This significant difference is attributed to the smaller characteristic length of the channel through which the refrigerant flows, as well as the 38 % lower flow velocity and is the main reason for differences (between HTHP A and HTHP B) in the overall heat transfer coefficient.

In summary, the overall heat transfer coefficients show the same behaviour in the condenser and a comparable order of magnitude, except for the operation points where the CHC is used, which leads to a smaller logarithmic medium temperature ($T_{sink,out} = 110$ °C).

The evaluation of the evaporator is shown on the right-hand side of Fig. 10. U_{evap} shows, in principle, the same behaviour for both systems.

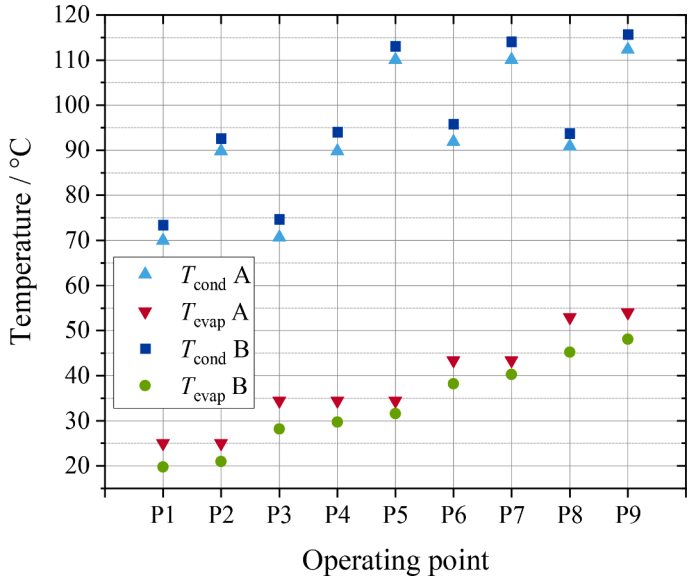

Fig. 9. Evaporation and condensation temperatures for different operation points.

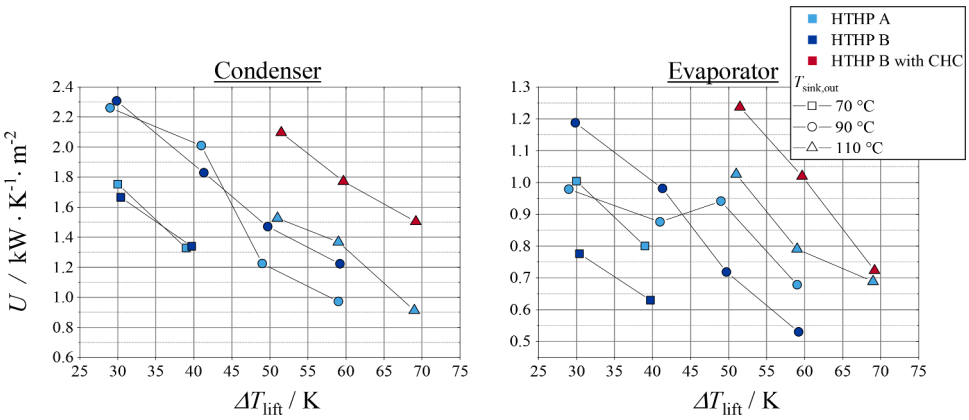

Fig. 10. Overall heat transfer coefficient as a function of the temperature lift for condenser and evaporator.

A decrease of U with rising temperature lift. However, the relative deviation between HTWP A and HTWP B is up to 31 % significantly higher than the condenser, neglecting the points where the CHC was used. In addition, operation points P1 to P4 show a lower overall heat transfer coefficient, and P5 to P9 a higher one for HTHP B. This is mainly due to the flow characteristics. There are only two data points for HTHP A where *Re* exceeds the value in HTHP B. The average logarithmic medium temperature in HTHP B is 7.3 K, much higher than in HTHP A with 3.5 K. The comparable low overall heat transfer coefficient in operation points P1 to P4 can be explained with the, in the previous chapter introduced, distribution device used in evaporator B. As mentioned, a pressure drop of at least 1 bar is required to ensure a good heat transfer. This pressure drop is not given in these operation points due to a low refrigerant mass flow rate. Thus, the heat transfer is hindered by the uneven distribution of the phases in the evaporator.

The heat rate describes the utilisation of the available heat exchanger surface so that higher thermal energy can be transferred per square meter, which should lead to a higher overall heat transfer coefficient. Thus, it can be seen that the heat transfer characteristics are comparable but that the design of system A contains surface reserves, what leads to 56 % smaller $\dot{q}$-values. The heat losses must be evaluated and compared to characterize a heat exchanger and a heat pump system comprehensively. The corresponding heat losses in the compressors and condensers are calculated regarding Eqs. (5) and (11). The heat losses are presented in Fig. 11 and show an increasing trend with increasing temperature lift in HTHP B. The heat losses in condenser B have a maximum of 4 % in relation to the thermal output of the HTHP system. On average, the heat losses are 1.9 % for the entire measurement series. Generally, the impact of the significantly higher surface-to-volume ratio can be observed, resulting in considerably lower heat losses for HTHP B compared to HTHP A. The heat losses in the compressor are not solely dependent on the temperature lift; rather, the varying sink temperatures demonstrate their influence.

The results show that there are many influences on the heat transfer efficiency. But if the heat exchanger design of two different plants is identical regarding minimum temperature approach and temperature glides. In that case, the larger plant will exhibit a higher efficiency due to the surface volume ratio. This influence can also be seen in the compressors and allows the assumption that the heat losses in big-scale heat pump compressors always stay under 10 %.

3.1.2. *Compressor*

To compare the performance of the compressors, the isentropic and volumetric efficiency are calculated. Both are calculated using the mass flow rate of the refrigerant, so the assumption of the heat losses in the condenser is crucial to the calculated isentropic efficiency in HTHP A. That is why in Fig. 12, the efficiencies as a function of the pressure ratio are shown for heat losses in the condenser in the case of 5 % and 10 %.

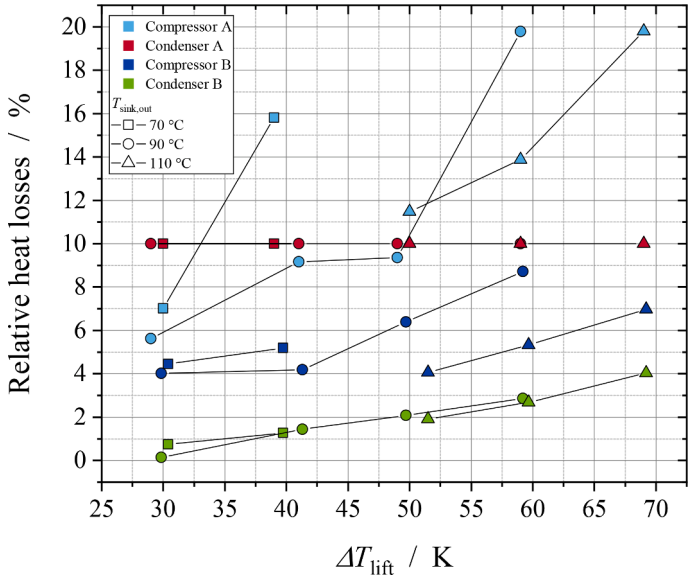

Fig. 11. Heat losses of compressor and condenser as a function of the temperature lift.

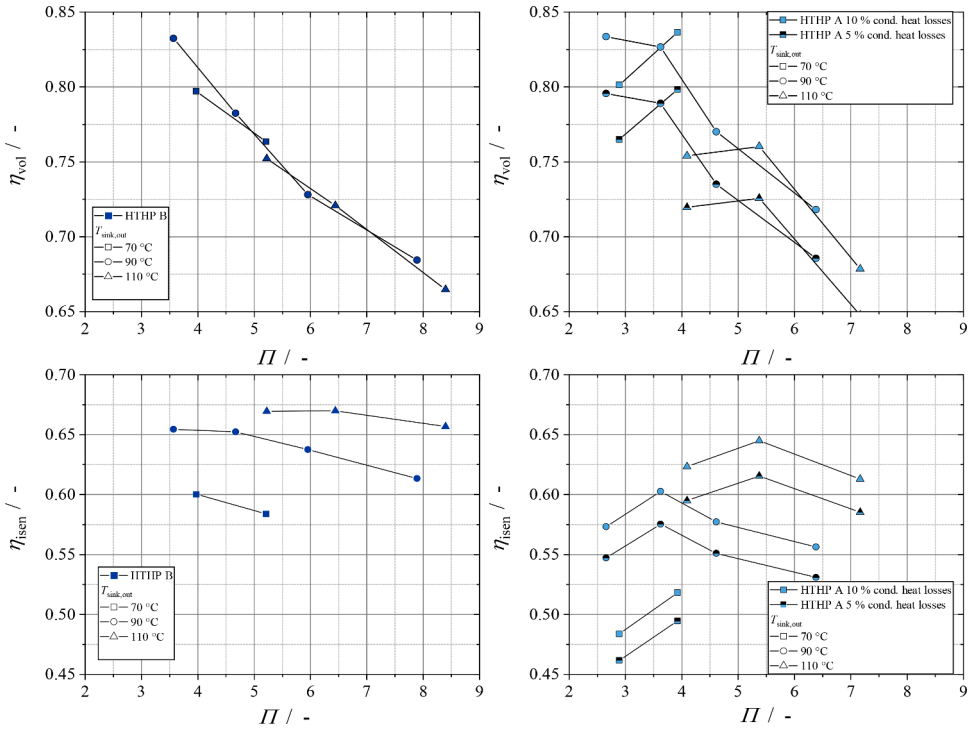

Fig. 12. Volumetric and isentropic efficiency as a function of the pressure ratio.

So, with decreasing heat losses, the refrigerant's mass flow rate and the volumetric and isentropic efficiency decrease.

The volumetric efficiency in the upper diagrams decreases with increasing pressure ratio, and both plants show a very similar order of magnitude and trend with increasing pressure ratio. The values of HTHP A have a higher variation around the trend line, which can result from the fact that each point was measured once. Another noteworthy observation is that HTHP B consistently exhibits higher pressure ratios at every operating point. This can be attributed to the lower evaporation pressure but with the same required heat sink temperature. Fig. 12 illustrates that the two compressors have a similar performance regarding the volumetric efficiency when the heat losses are assumed as 10 %. With heat losses of 5 % in the condenser, the volumetric efficiency decreases by 3.5 % in the medium.

Furthermore, the isentropic efficiency, which describes the ratio between the measured power draw and a theoretical isentropic one, is depicted in Fig. 12 in the lower diagrams. The results of HTHP A show a maximum at different pressure ratios, depending on the sink outlet temperature. This behaviour would likely occur in HTHP B, too, but due to the higher pressure ratios, the maximum is not observable in the measured range. The isentropic efficiency shows a higher difference between the two compressors. With heat losses of 10 % in the condenser, η_{isen} is on average 6 % lower than in HTHP B, with the 5 % assumption η_{isen} is on average 8.7 % lower than in HTHP B. Generally, compressor B operates more efficiently than compressor A. The differences can occur on the one hand due to a higher viscosity of oil for HTHP A and relatively lower friction losses compared to the total power draw for HTHP B.

3.2. Thermodynamic evaluation on the system level

On the system level, the most important value is the *COP*. But also heat losses play an important role for upscaling. Fig. 13 shows the *COP* as a function of the temperature lift ΔT_{lift} on the left hand. Due to the limitation in the mass flow rates and thus the varying temperature glide on the heat source side, the *COP* is shown on the right hand as a function of the evaporation temperature T_{evap}. The *COP* decreases with increasing temperature lift and increases with increasing evaporation temperature. The figure shows that only in one operation point, HTHP B shows a better efficiency (P2), and in one point, they are equal (P1). Compared to Fig. 7, these are the points where the water circuits show the lowest

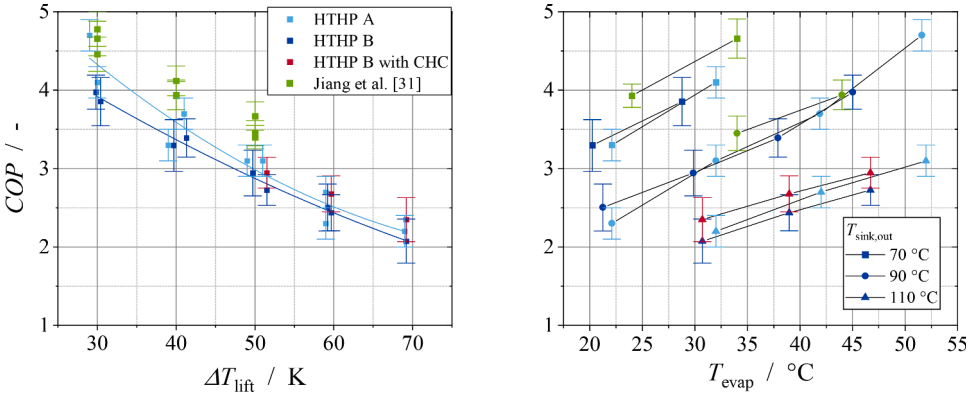

Fig. 13. *COP* as a function of the temperature lift (left) and evaporating temperature (right).

temperature differences, and the evaporation temperatures are nearly the same. In the context of the upscaling topic, another system besides HTHP A and B from the literature with a thermal output greater by a factor of 10, compared to HTHP B, is discussed in the following. Jiang et al. (2023) published a very efficient HTHP concept with different approaches regarding compressor and heat exchanger technologies. They achieved higher *COP*s with a very efficient turbo-compressor and superheating of about 1 K.

The measurement uncertainty of the *COP* is given with a maximum value of ± 0.22 for HTHP A and ± 0.25 for the HTHP system of Jiang et al. (2023). With the Gaussian error propagation, the uncertainty of the *COP* at operation point P9 (compare Fig. 5) leads to ± 0.20 in HTHP B. The maximum uncertainty of ± 0.33 *COP* can be recognised at point P1 due to the low temperature glide at the heat sink side the uncertainty of the temperature sensors has a large impact (see Table 3). Fig. 13 also compares the results of Jiang et al. (2023), representing a better *COP* in each operation point. However, it should be noted that comparing the results is limited due to another compressor concept and different superheating and subcooling operating conditions. To illustrate the influence of the evaporation temperature, on the right-hand side, the *COP* as a function of T_{evap} is shown. The figure also makes the influence of the CHC visible, with lower *COP*s without CHC, the *COP* increases over the *COP* of HTHP A. Also, the results of Jiang et al. (2023) show a good parity regarding the dependency of the evaporation temperature, and the figure shows the reason for the high *COP* values (higher evaporation temperature at the same temperature lifts). So, the trend of all three HTHPs is very similar and allows upscaling with a mean fluctuation rate of 0.68 for the *COP* as a function of the temperature lift. Neglecting the design effects like minimum temperature approach and temperature glide, the *COP* can be illustrated as function of the difference between the condensation temperature T_{cond} and the evaporation temperature T_{evap}, which is a common method in the literature, and is shown in Fig. 14. The figure shows a similar trend for all three HTHPs. The influences of the differences in the heat pump design become more visible especially between HTHP A and HTHP B. So HTHP B shows a better *COP* considering only the refrigeration circuit. This is also shown by the further increase of the *COP* presented by Jiang et al. (2023), but this can probably also be a result of the different plant designs.

Another option to evaluate the system performance is the ratio of the real *COP* and the ideal *COP*. Fig. 15 presents the calculated Carnot- and Lorentz-*COP*s. Due to the same heat source inlet and sink outlet temperatures, the Carnot-*COP* is equal in both HTHPs. The Lorentz-*COP* differs slightly but does not show a significant influence of the changing evaporation temperature (compare Fig. 13). So, the ratios in HTHP A are higher in most operating points than in HTHP B. The influence of the CHC suggests a relevant potential for future plant designs. Finally, the ratios are between 32 % and 43 % with an increasing *COP* ratio with increasing temperature lift. The comparison to an industrial plant in the following chapter shows that industrial Carnot-*COP* ratios are between 35 % and 60 % (Arpagaus et al., 2018).

The system analysis is finalised by the heat losses of the entire system, which are calculated as follows:

$$\dot{Q}_{loss} = \dot{Q}_{source} + P_{comp} - \dot{Q}_{sink} \tag{18}$$

Fig. 16 illustrates the relative heat losses referred to the thermal capacity of the heat sink as a function of the temperature lift. The heat losses of HTHP B increase with increasing temperature lift and with increasing sink outlet temperature. This is due to higher temperature difference to the ambient in the entire system.

The heat losses of HTHP A behave differently. So, no trend or dependence on a single variable can be identified. On average, the relative system heat losses are 15 % higher than in HTHP B. In summary, the heat losses of HTHP A are higher than in HTHP B, probably resulting from the different surface-to-volume ratio, because the isolation is comparable.

4. Scale effects

The presented results show different effects regarding the upscaling of an HTHP from 11 kW to 35 kW thermal capacity. It is necessary to distinguish between scale effects and design effects. The design effects like minimum temperature approach and temperature glide in the heat exchangers influence the system performance but can be adapted in every scale. The parameters to be observed for a scale-up of heat exchangers are the optimal heat transfer, realized exemplarily with a distribution device and the lower heat losses. In this context, the system performance of HTHP A is better or equal in most operating points, what shows the significant influence of the temperature glide and ΔT_{MITA}. Neglecting these design effects, the performance of the upscaled heat exchanger will be better due to relatively lower heat losses.

The analysis of the compressor shows that the isentropic efficiency of compressor B is higher, which probably is due to the lower viscosity of the oil and relatively lower friction losses. In sum, it is possible to use the experimental results of a HTHP and use them for a scale-up to a higher order of magnitude. Based on this conclusion, over 200 data points, firstly experimental data of different test plants (Arpagaus and Bertsch, 2019; Jiang et al., 2023; Fleckl et al., 2015; Helminger et al., 2016; Mateu-Royo et al.; Reißner; Moisi and Rieberer, 2017; Noack, 2016; Huang et al., 2017; Zhang et al., 2017; Xiaohui et al., 2014; Wemmers et al., 2017; Bobelin, 2012; Assaf et al., 2010; Wilk et al., 2016; Lee et al., 2017; Fukuda et al., 2014; Chamoun et al., 2012; Yamazaki and Kubo, 1985) and secondly data of industrial heat pumps, which were summarized by Arpagaus et al. (2018), are used to prove this phenomenon. Fig. 17 illustrates these different operation points of laboratory test plants as well as industrial serial products of other manufacturers. The technologies also differ in using internal heat exchangers, refrigerant, compressor technology (e.g., reciprocation, screw, and turbo compressor) and scale. Nevertheless, the considered heat pumps show the same trend, namely a decrease of the *COP* with increasing temperature lift.

The red curves represent the Carnot-*COP* ratio curve for a heat sink outlet temperature of 100 °C as a function of the temperature lift to classify the individual operating points regarding their *COP* ratio. A reasonable assumption for low-fidelity models would be to use a COP that is 45 % of the Carnot-*COP* for a set of operating conditions.

The influences of the different scales as well as other boundary conditions, have an impact on the *COP*. So, the Carnot approach can be

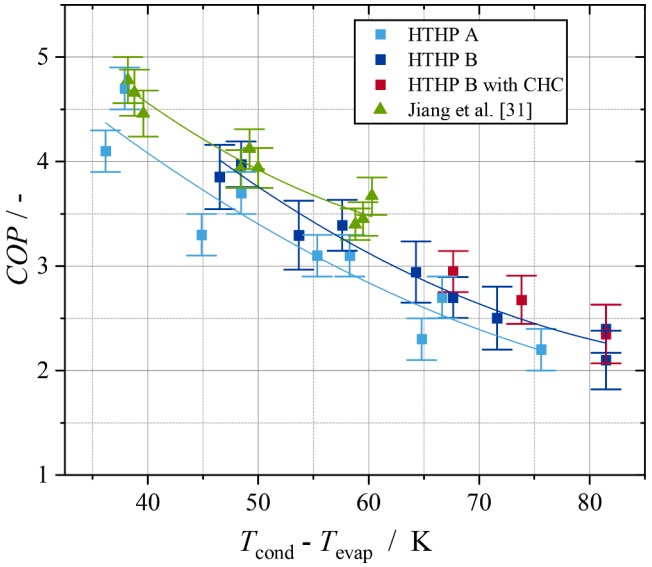

Fig. 14. COP as function of the difference between T_{cond} and T_{evap}.

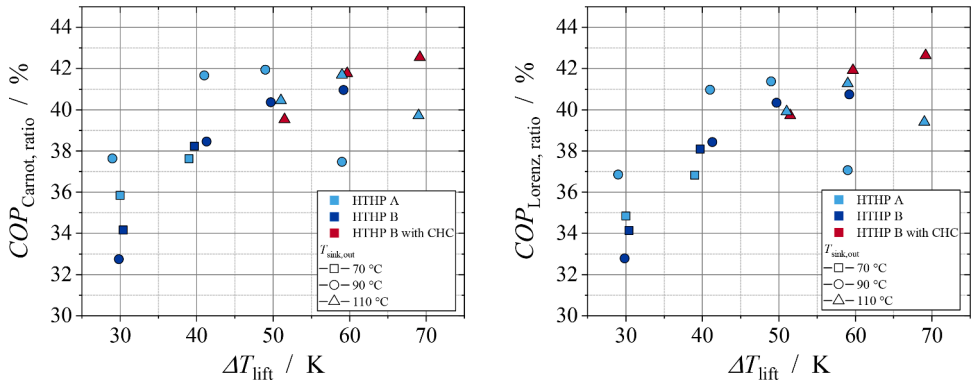

Fig. 15. *COP* ratio as a function of the temperature lift.

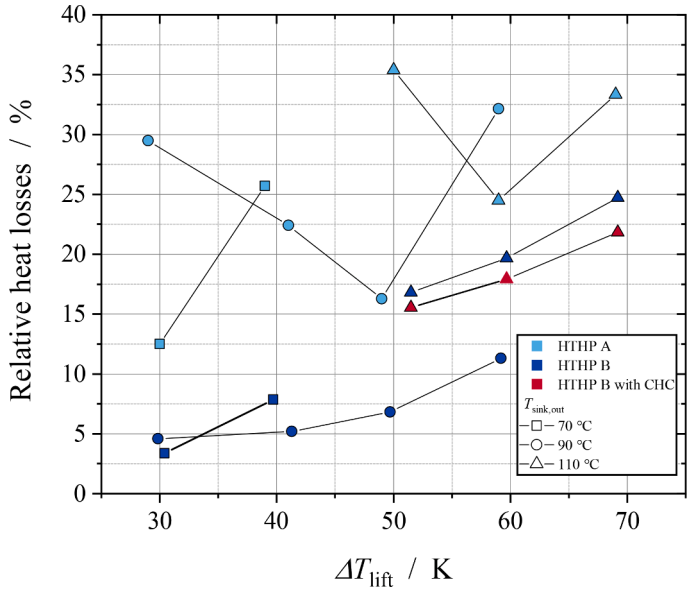

Fig. 16. System heat losses as a function of the temperature lift.

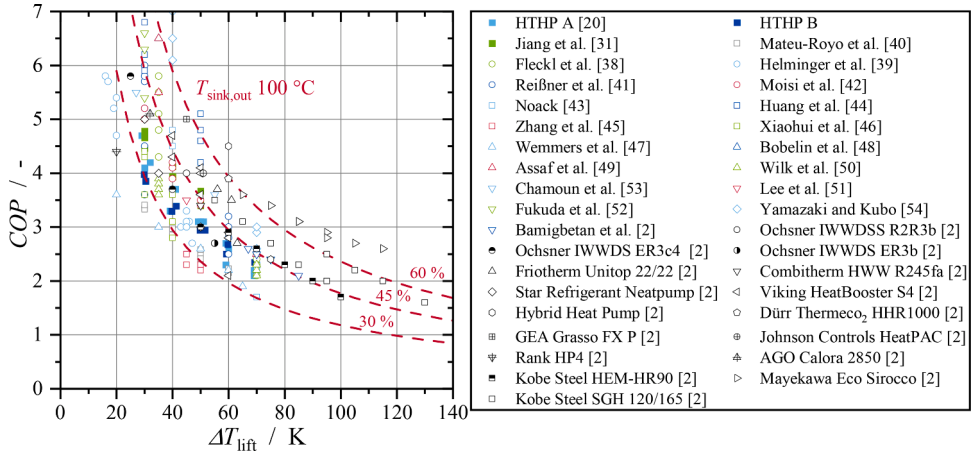

Fig. 17. *COP* as a function of the temperature lift of experimental and industrial plants from literature.

used as a reference for techno-economic and system analyses, where the design of a specified HTHP is not the focus. Nevertheless, it is necessary to include the exact boundary conditions in the calculations for a detailed system and economic analysis.

5. Conclusions

This study compared two laboratory high-temperature heat pumps (HTHPs) running with R1233zd(E) in a wide range of operation points regarding component and system aspects to make generally valid

statements about upscaling effects of laboratory heat pumps. The HTHP A, presented by Arpagaus and Bertsch (2019) and Arpagaus et al. (2018b), has a thermal capacity of about 11 kW, and the HTHP B (Jeßberger et al., 2022a, 2022b) has a thermal capacity of 35 kW leading to a scale-up factor of 3.2.

The heat exchangers show some differences regarding the overall heat transfer coefficient (e.g., large surface reserves in the heat exchangers lead to 3 K to 5 K smaller approach temperature differences in the heat pump with lower thermal capacity), the heat losses, temperature differences and the flow characteristics. While the flow characteristics and heat losses are better in the larger setup, the temperature glides and minimum temperature approaches in the smaller plant led to higher system performance.

It was necessary to distinguish between design and scale-up effects. The pinch points and temperature glides can be influenced by the relative component sizing, the scaling effects like 15 % higher heat losses in the smaller plant are probably due to a larger ratio of the surface for heat loss to the heating capacity. Interpreting these results, the larger setup promises a higher efficiency with a similar design.

This phenomenon can also be seen with the compressor. Due to a different power draw to friction ratio, the larger HTHP B shows better volumetric (0 % to 3.5 % higher) and isentropic (6 % to 8.7 % higher) efficiencies, depending on the heat losses assumed for condenser A. But these results can also be influenced by different lubricant oil selections. On the system level, the smaller setup shows in most of the operation points a better *COP,* resulting from the design effects. Considering the *COP* as a function of the evaporation temperature, the efficiencies are on a similar trendline, and the influence of the heat source temperature glide on the system performance can be shown. The used cylinder head cooling in the larger unit promises big potential for further studies to improve the system and component performance.

To further evaluate the upscaling results and the behaviour of the *COP* with increasing temperature lift, over 200 data points of industrial HTHP and research projects were analysed.

Using these data points, a reasonable assumption for low-fidelity models, for the integration of HTHPs into energy systems or industrial processes, would be to use a *COP* that is 45 % of the Carnot-*COP* for a set of operating conditions.

The limitations of the presented study lie in the focus on one single refrigerant, the specific type of compressor and pure measurements under laboratory conditions. In order to take these limitations into account, field data from industrial systems with different compressor types and refrigerants were also analysed and compared with the results. The study showed the possibility for a scale-up of laboratory HTHPs with a trend to a better efficiency of larger scales and points out important process and component parameters for a comparison (e.g., *COP, U*, heat losses, η_{isen}, η_{vol}, *COP* ratios).

In further work, the cylinder head cooling will be evaluated regarding optimization of the system performance and plant lifetime. The influence of the high-temperature operation on the oils and refrigerants will be investigated and based on the presented data set of the heat pump performance a correlation for the *COP* as function of sensitive parameters will be developed.

CRediT authorship contribution statement

Jaromir Jeßberger: Conceptualization, Data curation, Formal analysis, Investigation, Methodology, Validation, Visualization, Writing – original draft, Writing – review & editing. **Cordin Arpagaus:** Conceptualization, Data curation, Methodology, Validation, Writing – review & editing. **Florian Heberle:** Conceptualization, Funding acquisition, Methodology, Project administration, Resources, Supervision, Writing – review & editing. **Leon Brendel:** Conceptualization, Methodology, Writing – review & editing. **Stefan Bertsch:** Funding acquisition, Project administration, Resources, Supervision. **Dieter Brüggemann:** Funding acquisition, Project administration, Supervision, Writing – review & editing.

Declaration of competing interest

The authors declare that they have no known competing financial interests or personal relationships that could have appeared to influence the work reported in this paper.

Acknowledgments

The authors gratefully acknowledge the Bavarian State Ministry of Science and Arts within the framework of the "Geothermal Alliance Bavaria" project for funding. The authors further gratefully acknowledge the financial support of the Swiss Federal Office of Energy (SFOE) (SWEET project DeCarbCH www.sweet-decarb.ch, Annex 58 HTHP-CH with contract number SI/502336-01) and the Swiss National Science Foundation (SNSF) (Bridge Discovery project with grant number 203645).

Funded by the Deutsche Forschungsgemeinschaft (DFG, German Research Foundation) – 491183248. Funded by the Open Access Publishing Fund of the University of Bayreuth.

References

Adamson, K.-M., Walmsley, T.G., Carson, J.K., Chen, Q., Schlosser, F., Kong, L., Cleland, D.J., 2022. High-temperature and transcritical heat pump cycles and advancements: a review. Renew. Sustain. Energy Rev. 167 https://doi.org/10.1016/j.rser.2022.112798.

Arpagaus, C., Bertsch, S., 2019. Experimental results of HFO/HCFO refrigerants in a laboratory scale HTHP with up to 150°C supply temperature. In: 2nd Conference on High Temperature Heat Pumps.

Arpagaus, C., and Bertsch, C., Experimenteller Vergleich von R1224yd(Z) und R1233zd (E) n einer Hochtemperatur-Wärmepumpe, KI Kälte, 03, 2020 [German].

Arpagaus, C., Bertsch, S., 2021. Experimental Comparison of HCFO and HFO R1224yd (Z), R1233zd(E), R1336mzz(Z), and HFC R245fa in a high temperature heat pump up to 150°C supply temperature temperature heat pump up to 150°C supply temperature. In: International Refrigeration and Air Conditioning Conference vol. 2611.

Arpagaus, C., Bless, F., Uhlmann, M., Büchel, E., Frei, S., Schiffmann, J., Bertsch, S., 2018b. High temperature heat pump using HFO and HCFO refrigerants - System design, simulation, and first experimental results. In: International Refrigeration and Air Conditioning Conference. Paper 1875.

Arpagaus, C., Bless, F., Uhlmann, M., Schiffmann, J., and Bertsch, S., High Temperature Heat Pumps: market Overview, State of the Art, Research Status, Refrigerants, and Application Potentials, International Refrigeration and Air Conditioning Conference, 2018.

Arpagaus, C., Kuster, R., Prinzing, M., Uhlmann, M., Büchel, E., Frei, S., Schiffmann, J., Bertsch, S., 2019. High temperature heat pump using HFO and HCFO refrigerants - System design and experimental results. In: 25th IIR International Congress of Refrigeration (ICR.

Arpagaus, C., Prinzing, M., Bless, F., Uhlmann, M., Schiffmann, J., and Bertsch, S.S High temperature heat pumps - Theoretical study on low GWP HFO and HCFO refrigerants, in IIR International Congress of Refrigeration, 25th, 4254–4261, 10.18462/iir.icr.2019.259.

Assaf, K., Zoughaib, A., Sapora, E., Peureux, J., Clodic, D., 2010. Experimental simulation of a heat recovery heat pump system in food industries. In: International Refrigeration and Air Conditionig Conference.

Bamigbetan, O., Eikevik, T.M., Nekså, P., Bantle, M., 2017. Review of vapour compression heat pumps for high temperature heating using natural working fluids. Int. J. Refriger. 80 https://doi.org/10.1016/j.ijrefrig.2017.04.021.

Bamigbetan, O., Eikevik, T.M., Nekså, P., Bantle, M., Schlemminger, C., 2018. Theoretical analysis of suitable fluids for high temperature heat pumps up to 125°C heat delivery. Int. J. Refriger. 92 https://doi.org/10.1016/j.ijrefrig.2018.05.017.

Bobelin, D., 2012. Experimental results of a newly developed very high temperature industrial heat pump (140°C) Equipped with scroll compressors and working with a new blend refrigerant. In: International Refrigeration and Air Conditioning Conference.

Chamoun, M., Rulliere, R., Habschill, P., Peureux, J., 2012. Experimental investigation of a new high temperature heat pump using water as refrigerant for industrial heat recovery. In: International Refrigeration and Air Conditioning Conference.

Chen, T., Kyung Kwon, O., 2022. Experimental analyses of moderately high-temperature heat pump systems with R245fa and R1233zd(E). Energy Eng. 119, 6. https://doi.org/10.32604/ee.2022.021289.

climalife, Product data sheet solstice® zd [German].

Decorvet, R., Wärmepumpen ohne Grenzen, in 7. Internationaler Großwärmepumpen Kongress [German].

Deutsches Institut für Normung e.V., 1999. Grundlagen Der Meßtechnik: Teil 4: Auswertung von Messungen Meßunsicherheit. Beuth Verlag GmbH, Berlin. ICS 17.020, DIN 1319-4 [German].

DThermX (SWEP International AB).
European Union: COUNCIL REGULATION (EEC) No 594/91 of 4 March 1991 on substances that deplete the ozone layer (1991).
European Union: Regulation (EU) No 517/2014 OF THE EUROPEAN PARLIAMENT AND OF THE COUNCIL of 16 April 2014 on fluorinated greenhouse gases and repealing Regulation (EC) No 842/2006 (2014).
Fleckl, T., Wilk, V., and Hartl, M., Effiziente Abwärmenutzung durch Hochtemperaturwärmepumpen in der Industrie (2015) [German].
Frate, G.F., Ferrari, L., Desideri, U., 2019. Analysis of suitability ranges of high temperature heat pump working fluids. Appl. Therm. Eng. 150 https://doi.org/10.1016/j.applthermaleng.2019.01.034.
FUCHS, Safety data sheet, BSE85K (2020) [German].
Fukuda, S., Kondou, C., Takata, N., Koyama, S., 2014. Low GWP refrigerants R1234ze(E) and R1234ze(Z) for high temperature heat pumps. Int. J. Refriger. 40 https://doi.org/10.1016/j.ijrefrig.2013.10.014.
Hamacher, T., Industriewärmepumpe zur direkten Dampferzeugung, in DKV Tagungsband 2022, IV 13.
Hassan, A.H., Corberán, J.M., Ramirez, M., Trebilcock-Kelly, F., Payá, J., 2022. A high-temperature heat pump for compressed heat energy storage applications: design, modeling, and performance. Energy Rep. 8 https://doi.org/10.1016/j.egyr.2022.08.201.
Helminger, F., Kontomaris, K., Pfaffl, J., Hartl, M., and Fleckl, T., Hochtemperatur Wärmepumpen Messergebnisse einer Laboranlage mit HFO-1336MZZ-Z bis 160°C Kondensationstemperatur (2016) [German].
Høeg, A., Løver, K., Asphjell, T., Lümmen, N., 2023. Performance of a new ultra-high temperature industrial heat pump. In: 14th IEA Heat Pump Conference. Chicago, Illinois, 15-18 May.
Huang, M., Liang, X., Zhuang, R., 2017. Experimental investigate on the performance of high temperature heat pump using scroll compressor. In: 12th IEA Heat Pump Conference. Rotterdam.
International Energy Agency, Application of Industrial Heat Pumps: EA Industrial Energy-related Systems and Technologies Annex 13; IEA Heat Pump Programme Annex 35; Final Report Part 1 (2014).
IPCC, Climate Change 2014: synthesis Report. Contribution of Working Groups I, II and III to the Fifth Assessment Report of the Intergovernmental Panel on Climate Change (Geneva, Switzerland, 2014).
Jeßberger, J., Heberle, F., Brüggemann, D., 2022a. Integration of high temperature heat pumps into geothermal systems, in EGC 2022. European Geothermal Congress.
Jiang, J., Hu, B., Wang, R.Z., Deng, N., Cao, F., Wang, C.-C., 2022. A review and perspective on industry high-temperature heat pumps. Renew. Sustain. Energy Rev. 161 https://doi.org/10.1016/j.rser.2022.112106.
Jiang, J., Hu, B., Wang, R.Z., Ge, T., Liu, H., Zhang, Z., Zhou, Y., 2023. Experiments of advanced centrifugal heat pump with supply temperature up to 100°C using low-GWP refrigerant R1233zd(E). Energy 263. https://doi.org/10.1016/j.energy.2022.126033.
Khalid, H., Uzair, S., Ahrens, M.U., Ren, S., Ganesan, P., Tolstorebrov, I., Arshad, A., Said, Z., Hafner, A., Wang, C.-C., Wang, R., Eikevik, T.M., 2023. Potential evaluation of integrated high temperature heat pumps: a review of recent advances. Appl. Therm. Eng. 230 https://doi.org/10.1016/j.applthermaleng.2023.120720.
Jeßberger, J., Heberle, F., Brüggemann, D., 2022b. Integration von Hochtemperatur-Wärmepumpen in erneuerbare Energiesysteme, in DKV Tagungsband 2022, AA IV 19 [German].
Konstantinos Kontomaris: HFO-1336mzz-Z: high temperature chemical stability and use as a working fluid in organic rankine cycles, in international refrigeration and air conditioning 2014.
Längauer, A., Adler, B., 2023. High temperature test results and application cases of a rotation heat pump. In: 14th IEA Heat Pump Conference. Chicago, Illinois, 15-18 MayPaper 413.
Lee, G., Lee, B., Cho, J., Ra, H., Baik, Y., Shin, H., Lee, Y., 2017. Development of steam generation heat pump through refrigerant replacement approach. In: 12th IEA Heat Pump Conference. Rotterdam.
Mateu-Royo, C., Navarro-Esbri, J., Mota-Babiloni, A., Amat-Albuixech, M., Moles, F., 2019. Thermodynamic analysis of low GWP alternatives to HFC-245fa in high-temperature heat pumps HCFO-1224yd(Z), HCFO-1233zd(E) and HFO-1336mzz(Z). Appl. Therm. Eng. 152 https://doi.org/10.1016/j.applthermaleng.2019.02.047.
Mateu-Royo, C., Navarro-Esbrí, J., Mota-Babiloni, A., Molés, F., and Amat-Albuixech M. Experimental exergy and energy analysis of a novel high-temperature heat pump with scroll compressor for waste heat recovery, Appl. Energy 253, 10.1016/j.apenergy.2019.113504.
Moisi, H., and Rieberer, R., Refrigerant selection and cycle development for a high temperature vapor compression heat pump, 12th IEA heat pump conference, 2017.
Noack, R., Entwicklung einer Hochtemperatur-Wärmepumpe für Nutztemperaturen über 120°C, in DKV Tagungsband 2016 [German].
Reißner, F., Entwicklung eines neuartigen Hochtemperatur-Wärmepumpensystems (Erlangen) [German].
Sun, J., Wang, Y., Qin, Y., Wang, G., Liu, R., Yang, Y., 2023. A Review of Super-High-Temperature Heat Pumps over 100°C. Energies. (Basel) 16 (12). https://doi.org/10.3390/en16124591.
Shah, N.N., Cotter, D., and Hewitt, N.J., 2019. Overview on HCFO-R1233ZD(E) use for high temperature heat pump application, in 25th IIR International Congress of Refrigeration (ICR 2019), 286, 10.18462/iir.icr.2019.0286.
Web of science, HTHP publications per year: 2010-2022. https://www.webofscience.com/wos/woscc/summary/fcbbd3c8-220f-4326-b820-8f0b93f15b2e-91701725/relevance/1. Accessed 15 June 2023.
Wemmers, A., van Haasteren, A, Kremers, P., van der Kamp, J., 2017. Test results R600 pilot heat pump. In: 12th IEA Heat Pump Conference. Rotterdam.
Veronika Wilk, Michael Hartl, Thomas Fleckl, Erich Widhalm, Franz Ramler, Gottfried Adelberger, Thomas Ciepiela, and Karl Ochsner sen.: Hochtemperatur-Wärmepumpe für Industrieanwendungen: prüfstandsmessungen und Systemsimulation, DKV-Tagung 2016, 2016 [German].
World Energy Council, Der europäische Wärmemarkt: überblick und Herausforderungen (2020) [German].
Xiaohui, Y., Yufeng, Z., Na, D., Chengmin, C., lijun, M., lipin, D., Yan, Z., 2014. Experimental performance of high temperature heat pump with near-azeotropic refrigerant mixture. Energy Build. 78 https://doi.org/10.1016/j.enbuild.2013.12.065.
Yamazaki, T., Kubo, Y., 1985. Development of a high-temperature heat pump. In: IEA Heat Pump Centre Newsletter.
Zhang, Y., Zhang, Y., Yu, X., Guo, J., Deng, N., Dong, S., He, Z., Ma, X., 2017. Analysis of a high temperature heat pump using BY-5 as refrigerant. Appl. Therm. Eng. 127 https://doi.org/10.1016/j.applthermaleng.2017.08.072.